Controlling the Time Evolution of Electron-Nuclei Entanglement for Steering Vibronic Coherences Dynamics Induced by Short 1–2 fs Optical Pulses

Martin Blavier, Natalia Gelfand, R. D. Levine, and F. Remacle

Abstract Atto pulses allow controlling the charge migration and the spatio-temporal beating of the electronic density on a purely electronic time scale by tailoring the parameters of the pump pulse to excite specific electronic coherences. As the nuclei begin to move, the electronic and nuclear motions are entangled and the engineered electronic coherences can be usefully exploited for steering the vibronic density to specific products through the network of non adiabatic interactions. Three recent examples for which we demonstrate such a control by fully quantum dynamical computations are discussed. Two diatomic molecules, LiH and N_2 excited by a 2 fs deep UV pulse and the ultrafast structural Jahn-Teller rearrangement in CH_4^+. The entanglement between electronic and nuclear degrees of freedom arises from the optical excitation and from non adiabatic coupling induced by the nuclear motion. We provide insight of the coherence control mechanism by analyzing the time evolution of the entanglement using a singular valued decomposition (SVD) of the matricized wave function.

Authors Martin Blavier and Natalia Gelfand have equally contributed to this chapter.

M. Blavier · F. Remacle (✉)
Theoretical Physical Chemistry, RU MolSys, University of Liege, Liège, Belgium

Fritz Haber Research Center, Institute of Chemistry, The Hebrew University of Jerusalem, Jerusalem, Israel
e-mail: fremacle@uliege.be

N. Gelfand
Fritz Haber Research Center, Institute of Chemistry, The Hebrew University of Jerusalem, Jerusalem, Israel

R. D. Levine
Fritz Haber Research Center, Institute of Chemistry, The Hebrew University of Jerusalem, Jerusalem, Israel

Department of Chemistry and Biochemistry, Department of Molecular and Medical Pharmacology, David Geffen School of Medicine, University of California, Los Angeles, CA, USA

L. Argenti et al. (eds.), *Proceedings of the 8th International Conference on Attosecond Science and Technology*, Springer Proceedings in Physics 300,
https://doi.org/10.1007/978-3-031-47938-0_9

Keywords Attosecond molecular quantum dynamics · Time-resolved electron-nuclei entanglement in molecules · Schmidt rank · Singular value decomposition · Matricization of the wave function

1 Introduction

Recently, short optical atto (as) and few femtosecond (fs) pulses have provided new insights into ultrafast dynamics and charge migration in molecular systems and in solids [1–10].

The novel feature brought by such short pulses is that they lead to an initial state that is a superposition of the different electronic states that fall within the broad pulse energy bandwidth. By tuning the pulse parameters, one can engineer electronic coherences between selected electronic states and control the charge migration and the spatio-temporal beating of the electronic density on a purely electronic time scale [11–13]. As the nuclei begin to move, the electronic and nuclear motions become entangled and the engineered electronic coherences can be usefully exploited for steering the vibronic density through the network of non adiabatic interactions to specific products [14–16].

Entanglement arises when the wave function of two subsystems cannot be written as a single product of separable terms depending each of the coordinates of one of them [17, 18]. It is an important property of multipartite systems that plays an essential role in quantum information and quantum communication [19]. Entanglement also plays an important role in quantum dynamics. Non adiabatic interactions between electronic states driven by nuclear motion and the breakdown of the Born and Oppenheimer approximation have been long recognized as a source of electron-nuclei correlation leading to the entanglement of the vibronic wave function [20–25]. One can entangle vibrational modes in a polyatomic molecule, [26] or scattering channels in chemical reactions [27, 28]. Attopulse pump probe schemes were used recently to probe the entanglement between the cation and the leaving photoelectron, in the molecular ion H_2^+ [29, 30] and in atoms [31].

Here, we focus on the entanglement of electrons and nuclei brought by exciting molecules to a superposition of several electronic states with short optical pulses and on the special role of the entanglement for the control of the ensuing non adiabatic quantum dynamics leading to the products [32, 33]. We analyze the time evolution of the entanglement between nuclear and electronic degrees of freedom using singular value decomposition (SVD) of the wave function rewritten as a matrix and known as matricizing [34]. Three cases are investigated: the quantum dynamics on coupled electronic states of two diatomic molecules, LiH and N_2, photoexcited by short UV 2 fs pulses and the multi-dimensional quantum dynamics of the Jahn Teller ultrafast structural rearrangement of the molecular cation CH_4^+ upon strong field ionization of the neutral [35].

2 Quantification of the Time Evolution of Electron-Nuclei Entanglement in Molecules

The entanglement of the wave function of a multipartite system can be quantified using its Schmidt rank [17, 18]. The Schmidt rank is the minimum number of separable product terms necessary to describe the wave function. When the wave function can be described as a single product of separable terms, the system is not entangled and its Schmidt rank is equal to 1. When more than one term is necessary, the wave function is entangled and its Schmidt rank is larger than 1.

2.1 Quantum Vibronic Dynamics in Coupled Electronic States

In the quantum dynamical simulations reported below, we expand the wave function in a double sum of products of a nuclear wave function and an electronic state. The basis of nuclear wave functions is taken to be a set of N_g door functions localized at equally spaced grid points, $|g_n\rangle$, along the nuclear coordinate. The electronic wave function is described in the basis of a band of N_e adiabatic states, $|e_i\rangle$. At the end of the broad in energy exciting pulse, the wave function is a superposition separable products, $|g_n\rangle|e_i\rangle$, the Born Huang expansion

$$|\Psi(t)\rangle = \sum_{n=1}^{Ng} \sum_{i=1}^{Ne} c_{ni}(t)\, |g_n\rangle\, |e_i\rangle \tag{1}$$

The complex coefficients, $c_{ni}(t)$, are obtained by solving the time-dependent Schrödinger equation:

$$i\hbar \frac{d}{dt}\mathbf{c} = \mathbf{H}(t)\mathbf{c} \tag{2}$$

where $\mathbf{c}$ is the vector of the $N_g.N_e$ coefficients $c_{ni}(t)$. $\mathbf{H}(t)$ is the matrix of the molecular Hamiltonian in the separable basis $\{|g_n\rangle|e_i\rangle\}$:

$$\mathbf{H}_{ni,mj}(t) = -\frac{1}{2}\mathbf{T}_{ni,mj}\delta_{ij} + \mathbf{V}_{ni,nj}\delta_{nm}\delta_{ij} - \mathbf{E}(t)\mu_{ni,mj}\delta_{nm} - \left(\frac{1}{i}\tau_{ni,mj}\delta_{mn}.\mathbf{p}_{mi,nj}\right) \tag{3}$$

where *n,m* are the index of the grid points and *i,j* the index of the electronic states. The first two terms on the rhs are the kinetic and potential energies of the nuclei. The interaction with the time-dependent electric field of the short pulse is described in the dipole approximation (third term). $\mathbf{E}(t)$ is the time profile of the electric field defined from the derivative of the vector potential confined in a short Gaussian envelope:

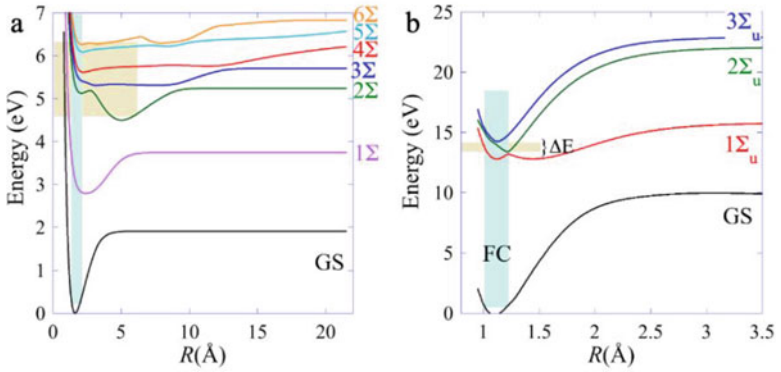

Fig. 1 (**a**) Potential energy curves of the 7 lowest Σ adiabatic states of the LiH molecule included in the computations [36]. (**b**) Potential energy curves of the 4 lowest electronic adiabatic states of N_2 included in the computation [37]. The Franck-Condon (FC) region is indicated in shaded blue and the energy band width, ΔE, of the short pulse in shaded yellow

$$\mathbf{E}(t) = -\frac{d\mathbf{A}(t)}{dt} = \left(\hat{\mathbf{e}} f_0\right) \exp\left(\frac{-(t-t_0)^2}{2\sigma^2}\right)\left(\cos\left(\omega\,(t-t_0)+\phi\right) + \frac{\sin(\omega(t-t_0)+\phi)(t-t_0)}{\omega\sigma^2}\right) \tag{4}$$

The last term in Eq. (3) describes the non adiabatic interactions driven by the nuclear motion. The last two term terms in Eq. (3) are the source of entanglement between electrons and nuclei as the dynamics unfolds. The excitation by the short pulse inherently entangles electron and nuclei because it promotes the ground vibrational state of the ground electronic state (GS) to a superposition of several excited electronic states (Fig.1).

As we show below, as long as all the wave packets on each excited electronic state remain localized in the Franck-Condon (FC) region, the wave function (Eq. (1)) is separable and the Schmidt rank is equal to 1. When the nuclei begin to move, the wave packets on each electronic state experience a different gradient which leads to the entanglement of the wave function, even in the absence of non adiabatic coupling.

2.2 *S Schmidt Rank and Compaction by Singular Value Decomposition of the Matricized Wave Function*

To analyze the time evolution of the entanglement, at each time step, we matricize the $N_g.N_e$ amplitude vector, $\mathbf{c}(t)$, into N_g x N_e rectangular matrix $\mathbf{C}(t)$, followed by a Singular Value Decomposition (SVD) [32, 33]. Since typically$N_g > N_e$, the matrix

$\mathbf{C}(t)$ has at most N_e singular values [38] and the matrix $\mathbf{C}(t)$ can be written as a sum of at most N_e separable terms:

$$\mathbf{C}(t) = \sum_{m}^{Ne} \sigma_m(t) \, |u_m\rangle \, (t). \left|v_m^{\dagger}\right\rangle (t) \tag{5}$$

The wave function will therefore have a maximum Schmidt rank equal to N_e.

In Eq. (5), $|u_m(t)\rangle$are the N_e left eigenvectors of the matrix $\mathbf{C}(t)$**,** $|v_m(t)\rangle$ are its right eigenvectors and $\sigma_m(t)$ are the singular values. The singular values are real and the singular vectors are complex. The vectors $|u_m(t)\rangle$ are the nuclear singular vectors, they have components on the grid basis function only. The vectors $|v_m(t)\rangle$ are the electronic singular vectors. They have components on the electronic states only.

$$|u_m(t)\rangle = \sum_{n=1}^{Ng} u_{nm}(t) \, |g_n\rangle \tag{6}$$

$$|v_m(t)\rangle = \sum_{i=1}^{Ne} v_{im}(t) \, |e_i\rangle \tag{7}$$

Using Eqs. (6) and (7), the Born-Huang amplitudes of Eq. (1) are a sum of N_e separable terms:

$$c_{ni}(t) = \sum_{m=1}^{Ne} \sigma_m(t) u_{nm}(t) v_{im}^{*}(t) \tag{8}$$

From Eq. (8), one sees that the normalization of the wave function is given by:

$$\mathrm{Tr}\left[\rho(t)\right] = \sum_{m=1}^{Ne} \sigma_m^2(t) = 1 \tag{9}$$

The exact expression given by Eq.(5) already provides a significant compaction of the wave function in at most N_e terms compared to the N_e . $N_g$terms of the Born-Hunag expansion Eq. (1):

$$|\Psi(t)\rangle = \sum_{m}^{N_e} \sigma_m(t) \, |u_m\rangle \, (t). \left|v_m^{\dagger}\right\rangle (t) \tag{10}$$

A further compaction can be obtained by ordering the singular values $\sigma_m(t)$ by decreasing values and retaining the $N_{\min}$ terms that provide an approximation of the wave function up to a certain threshold (for example of the normalization):

$$|\Psi(t)\rangle = \sum_{m}^{N_{\min}} \sigma_m(t)\,|u_m\rangle\,(t).\,\left|v_m^{\dagger}\right\rangle(t),\ N_{\min} < N_e \tag{11}$$

When$N_{\min}$ is smaller thanN_e, $\mathrm{Tr}[\rho(t)] < 1$. How well the value of $\mathrm{Tr}[\rho(t)]$ approaches unity can be used for estimating $N_{\min}$.

3 Dynamical Evolution of the Entanglement and of the Singular Components

We begin by comparing the time evolution of the Schmidt rank and of the entanglement in two diatomics: LiH and N_2, excited by short ≈ 2 fs UV pulses.

We show in Fig.2 the dynamics of the populations in the electronic states of the LiH molecule computed by solving the time-dependent Schrödinger equation for the Hamiltonian given by Eq. (3) for 7 coupled Σ electronic states, see Ref. [36] for curves of the transition dipoles and NAC couplings. The vibrational ground state (GS) is excited with a short UV pulse polarized towards the H atom along the molecular axis, so as to selectively access the Σ_2, Σ_4 states. The pulse has a carrier frequency of 5.5 eV and a Gaussian envelope with a Full Width at Half Maximum (FWHM) of 2 fs which corresponds to an energy bandwidth of

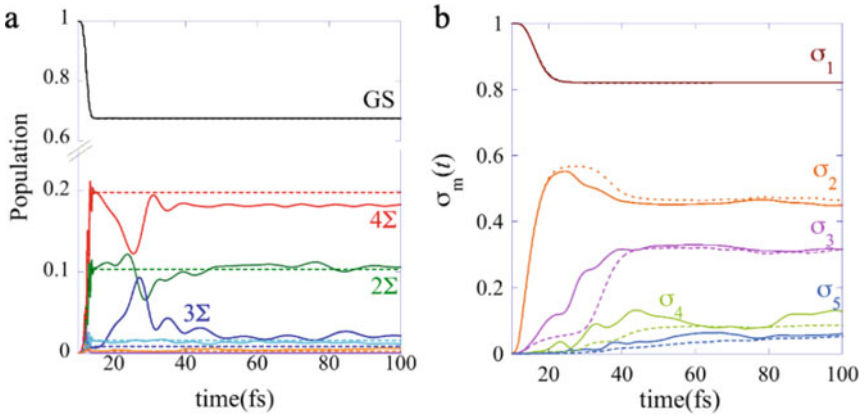

Fig. 2 (**a**) Dynamics of the populations of the adiabatic states in the LiH molecule, full lines NACon and dashed lines NACoff. The dynamics of the two computations is nearly identfical during the pulse. (**b**) singular values,$\sigma_m(t)$, computed by SVD after matricization of the wave function at each time step. Full lines NACon, dashed lines NACoff

1.84 eV. Two computations are carried out, one that includes the NAC term in the Hamiltonian (NACon, full lines) and one that does not (NACoff, dashed lines). The two computations differ significantly by the amount of population in the Σ_3 state, which is not significantly populated in the NACoff computation and is populated transiently in the NACon ones. In the NACoff computations, the populations in the electronic states are stationary after the pulse. By comparing the two curves, one see that towards the end of the pulse, non adiabatic interactions bring population to Σ_3 which is much less optically active than Σ_2 and Σ_4 for a polarization of the pulse towards the H atom. Already during and right after the pulse, there is extensive population exchange between these three states induced by NAC. After 50 fs, the populations are almost stationary as the wave packets proceed to dissociation on these three electronic states.

The time evolution of the singular values, $\sigma_m(t)$, obtained by SVD after the matricization of the wave function at each time step, are plotted in Fig. 2b for the two computations. During the first half of the pulse, the wave function remains separable and is described by a single term for both computations. The onset of nuclear motion is accompanied by the rise of a second component, that describes the exit of the wave packets of the FC region. In the NACoff computations, the time evolution of the entanglement is solely controlled by the superposition of electronic states built by the short pulse and the gradient differences between the electronic states accessed at the excitation step. As long the gradients on each potential curve remain similar, a second principal component suffices for describing the dynamics. In the NACon one, the second and third components rise earlier, as amplitude is transferred to the Σ_3 state by the NAC at the exit of the FC region. In LiH, we therefore observe an increase of the Schmidt rank (and of entanglement) as the nuclear motion sets in, at the exit of the FC region, in the first 50 fs of the dynamics. The increase is driven by the differences in the gradients of the potential curves of the states excited by the pulse and by the non adiabatic interactions, and primarily affects the $\sigma_2(t)$, $\sigma_3(t)$ and $\sigma_4(t)$ singular values plotted in Fig. 2b. On the other hand, in the NACoff computation, the increase is only driven by the difference of the gradient of the poettnial energy cures of these three states, with the result that in the first 50 fs of the dynamics, the increase of the entanglement is slower in the NACoff computation. Asymptotically, there is essentially no difference in the degree of entanglement between the NACon and the NACoff computation since the NAC is very small asymptotically.

Further insights are given by analyzing the components of the nuclear and electronic singular vectors on the grid and on the adiabatic electronic states respectively. Heatmaps of the components of the first four nuclear singular vectors are plotted in Fig. 3 for the NACon and the NACoff computations. The components of the electronic singular vectors are plotted in Fig. 4. The first nuclear singular vector is localized in the FC region (Fig. 3a). It corresponds to the largest singular value since 67% of the population remains in the GS after the pulse. Accordingly, the electronic singular vector is localized on the GS except during the first half of the pulse, when all the wave packets on the excited electronic states are still localized

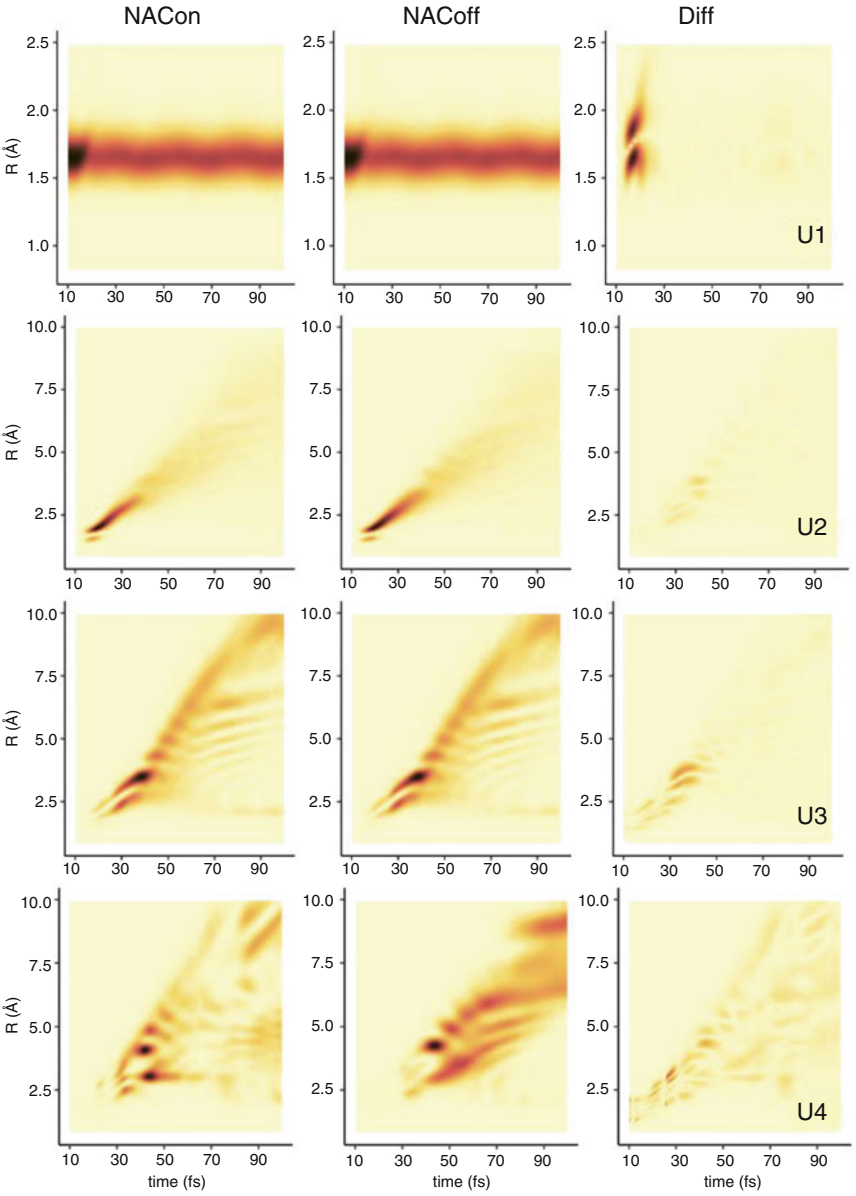

Fig. 3 Heatmaps of the localization of the first four nuclear singular vectors for the NACon computation (left) and the NACoff computation (middle). The weights at each grid point are multiplied by the principal values $\sigma_m^2(t)$. The difference between the unweighted nuclear singular vectors is shown in the right column to illustrate the role of the non adiabatic interactions

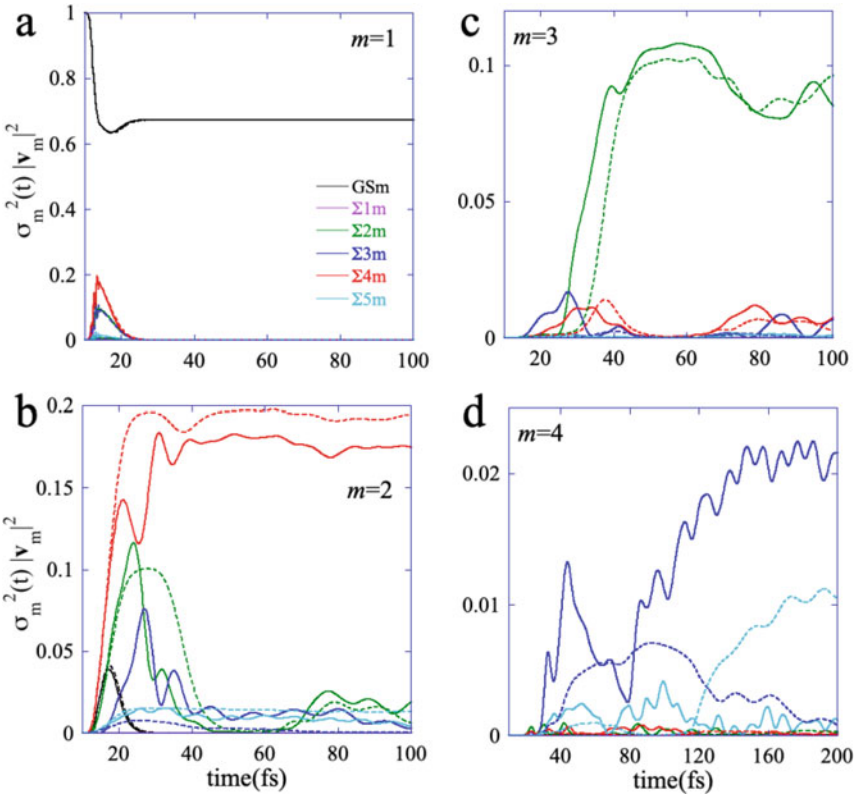

Fig. 4 Weights of the electronic singular vectors of the four largest principal components on the adiabatic electronic states. Full lines: NACon, dashes: NACoff. The weights $|v_{im}|^2$ are multiplied by the principal values $\sigma_m^2(t)$. Note the decrease by a more than an order of magnitude for $m = 4$, that localises on Σ_3 at long times in the NACon computation

in the FC region (Fig. 4a). Then, the electronic singular vector is also localized on the two most active electronic states, Σ_4 and Σ_2. The second principal value, $\sigma_2(t)$, begins to rise in the second half of the pulse (Fig. 2b). Right after the pulse, the second electronic singular vector, $\mathbf{v}_2$**,** has weights on several adiabatic states both in the NACon and in the NACoff computations. The effect of the $\Sigma_4 - \Sigma_3$ and $\Sigma_2 - \Sigma_3$ non adiabatic interactions is clearly seen in the weights of the three electronic singular vectors, $\mathbf{v}_2$, $\mathbf{v}_3$, $\mathbf{v}_4$ on the adiabatic electronic states, Fig. 4b, c, d respectively. In the NACon computation, $\mathbf{v}_2$, $\mathbf{v}_3$, $\mathbf{v}_4$ have a significant component on Σ_3 which is much smaller in the NACoff one. After the NAC region, beyond 50 fs, the second electronic singular vector, $\mathbf{v}_2$, localizes on Σ_4 and the third one, $\mathbf{v}_3$, on Σ_2. In the NACon computation, at long times the fourth electronic singular vector, $\mathbf{v}_4$, localizes on Σ_3 (not shown) while its localizes on Σ_5 in the NACoff

one. As discussed above, below 50 fs, the nuclear vectors are localized on several electronic states coupled by the NAC interactions while at longer times, they reflect the gradient of the potential energy curve on which the singular component is localized. This is clearly seen in the last column of Fig. 3 where we show the difference between the nuclear singular vectors computed for the NACon (first column) and the NACoff (second column).

In the case of the N_2 molecule, the short UV pulse has an excitation wavelength of 13.6 eV and a duration σ of 1.32 fs (FWHM of 1.18 eV) so as to selectively excite the two lowest Σ_u states (the lowest Rydberg state and the valence state, see Fig. 1b) below their dissociation asymptote. Unlike in LiH, the motion of the excited wave packet is bound and the lowest Rydberg state and the valence state are strongly coupled by NAC at the exit of the FC region. The population dynamics is plotted in Fig. 5a. The pulse builds a superposition of the lowest Rydberg state and the valence state. Right at the exit of the FC region, almost all the population of the Rydberg state is transferred to the shallow valence state. The Rydberg state is periodically repopulated each time the valence wave packet revisits the NAC region and comes back to the FC region, every 40 fs. Compared to the LiH case discussed above, this periodic evolution of the population in the two states leads to a rather different time evolution of the entanglement and of the Schmidt rank. The time evolution of the singular values $\sigma_m^2(t)$ is plotted in Fig.5b. Because of the strong non adiabatic interactions and of the very different gradients of the potential of the Rydberg and the shallow valence state, three singular values are needed to describe the wave function at all times. Their time evolution is non monotonic and reflects the periodic motion of the wave packet on the valence state. Each time the wave

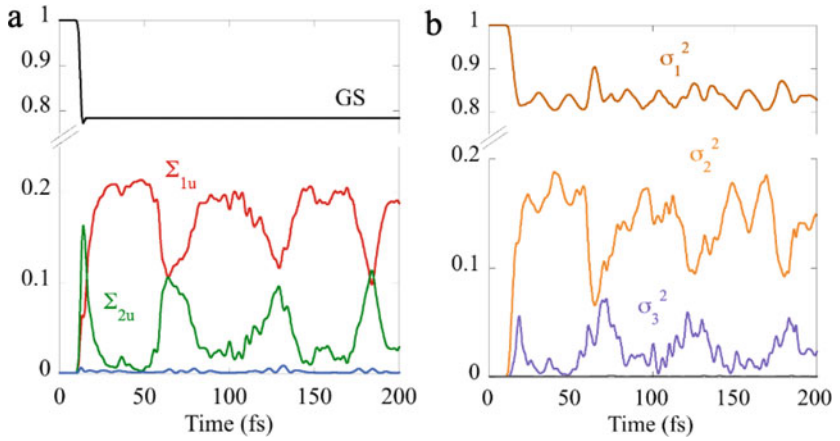

Fig. 5 (**a**) Dynamics of the populations in N_2 excited to the lowest Rydberg and valence states by a 2 fs UV pulse. (**b**) singular values, $\sigma_m(t)$, computed by SVD after matricization of the wave function at each time step

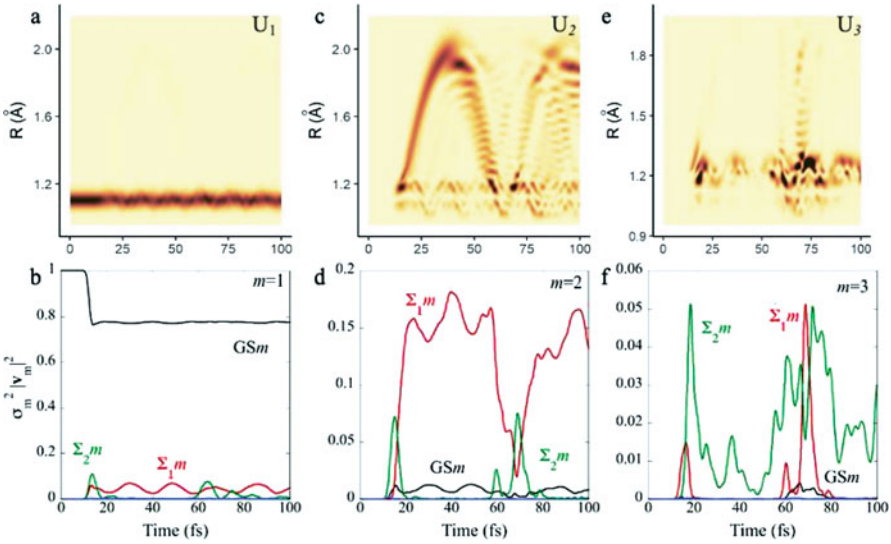

Fig. 6 Heatmaps of the nuclear singular vectors of the three largest principal components in N_2 (panels a, c, d). Corresponding composition of the electronic singular vectors on the adiabatic electronic states (panels b, d, f). The weights of the singular vectors are multiplied by $\sigma_m^2(t)$

packet on the valence state revisits the FC region there is a non monotonic variation of the $\sigma_1(t)$, $\sigma_2(t)$ and $\sigma_3(t)$ singular values: $\sigma_1(t)$ and $\sigma_3(t)$ increase and $\sigma_2(t)$ decreases. This non monotonic change is due to the fact that a larger fraction of the wave packet is localized in the FC region and therefore can be described by the first and third singular component. Indeed, the nuclear singular vector, U1, of the largest principal component is localized in the FC region as in LiH, Fig. 6a. But unlike in LiH, the first electronic singular vector, $\mathbf{v}_1$, has components on the valence and Rydberg states each time the wave packet revisits the NAC region (Fig. 6b). This periodic motion is reflected in the value of the largest singular value which rises when the wave packet passes through the NAC region (Fig. 5b). The second electronic singular vector, $\mathbf{v}_2$, is mainly localized on the valence state except in the NAC region where it has components on the Rydberg state (Fig. 6d). Accordingly, the localization on the second nuclear singular vector, U2, extends in at large R values which correspond to the shallow potential of the valence state (Fig. 6c). The third principal component is localized on the Rydberg state and has a very low weight except in the NAC region where its nuclear and electronic singular vectors acquire a weight on the valence state (Fig. 6e, f).

In both LiH and N_2 (Fig.2b and Fig.4b respectively), one can see that in the regions of non adiabatic interaction, the singular values go through an avoided crossing as a function of time.

4 Extending to More than One Nuclear Degree of Freedom: Ultrafats Dynamics of the Jahn-Teller Effect in the Methane Cation

Upon sudden ionization of the neutral, the methane cation undergoes an ultrafast structural rearrangement triggered by the Jahn-Teller effect. This ultrafast vibronic dynamics has been probed by attosecond High Harmonic Spectroscopy (HHS) by Marangos et al. [39, 40] who reported a strong isotope effect, larger than what is expected classically from the ratio of the reduced masses. Dynamical computations provided insights on the role of the non-adiabatic interactions between the three electronic states of the cation, D_0, D_1 and D_3 involved [35, 41–44]. We have shown [35, 44] using fully quantum dynamics on three coupled electronic states (D_0, D_1, D_2) and two nuclear coordinates (q_1, q_2) that electronic coherences involving the D_2 state are instrumental to yield the unusually strong isotope, whether the sudden ionization results from photoionization by a XUV pulse [44] or from strong field ionization as in HHS [35].

We report here on preliminary results analyzing the time evolution of the entanglement between electron and nuclear in the ultrafast dynamics of the methane cation driven by strong field ionization (SFI) of the neutral. Details of the computations can be found in Ref. [35]. A sketch of the 2-dimensional potential of the three states is plotted in Fig. 7a. For two nuclear coordinates and three electronic states, there are $N_e . N_{q1} . N_{q2} \approx 80{,}000$ separable product terms $(|g_{q1}\rangle|g_{q2}\rangle|e_i\rangle$ in the Born Huang expansion of the wave function (Eq. (1)). Since we have three subsystems, we recast the vector of the amplitudes into a 3-dimensional tensor $\mathbf{C}$ which we decomposed by High Order SVD [45].

$$C_{jki} = \sum_{s=1}^{Nq1} \sum_{t=1}^{Nq2} \sum_{r=1}^{Ne} \sigma_{rst} \mathbf{U}_{js} \mathbf{W}_{kt} \mathbf{V}_{ir} \tag{12}$$

where the indices j and k correspond to the grid points along $q1$ and $q2$ respectively and i is the index of the three electronic states. σ_{rst} are the (complex) values of the core tensor of the HOSV Decomposition [45]. $\mathbf{U}_{js}$ and $\mathbf{W}_{kt}$ are the nuclear singular vectors along the $q1$ and $q2$ coordinate respectively and $\mathbf{V}_{ir}$ the electronic singular vector. We show in Fig7b the dynamics of the populations in the three states of the cation D_0, D_1 and D_2, induced by sudden ionization with a strong IR field (2 10^{14} W/cm^2), as described in Ref. [35]. Compared to LiH and N_2, we obtain a massive compaction of the wave function when applying SVD to the wave function written as a tensor. The number of terms in Eq. (12) needed to recover 99% of the trace of the density matrix, Tr$[\rho(t)]$, is plotted in Fig. 7c. From 10 fs on, ≈2000 terms suffice, compared to 80,000 separable terms in the Born-Huang expansion.

The degree of compaction is even larger at short times, in the first few fs. The localization of the wave function at each grid point ($q1$, $q2$) on the three electronic

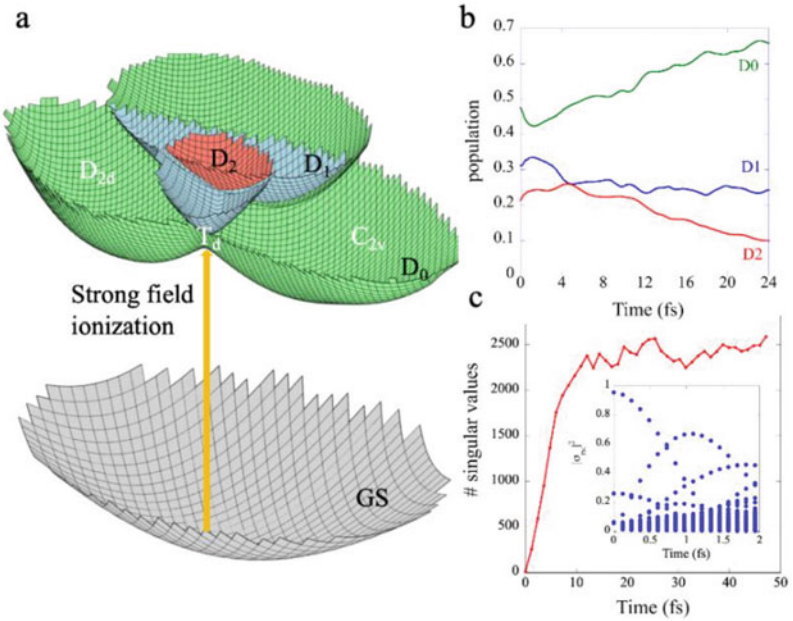

Fig. 7 (**a**) A schematic view of the 2 dimensional potentials of the three electronic states of the cation that are reached by string field ionization [35] (**b**) the time evolution of the populations on the three electronic states of the cation resulting from a sudden ionization process with a strong field of 2 10 ^{14} W/cm^2. (**c**) The number of singular terms in the HOSVD expansion needed to recover 99% of the trace of the density matrix for the first 50 fs of the dynamics. The inset shows the values of the elements of the core tensor for the first two fs

states is plotted in the top row of Fig. 8 at 0.85 fs. In the bottom row, we show the recovered localization on the grid obtained from the 193 separable terms necessary for accounting for 99% of the trace. One can see that the main patterns of the localization of the wave function on the three electronic states are well captured. The same is true at 1.7 fs (Fig. 9) for which 366 terms are needed. Work is in progress on the physical interpretation of the most important separable terms and on the analysis of the entanglement.

5 Conclusion

The matricization of the wave function vector followed by SVD provides an efficient way to follow the time evolution of the Schmidt rank of the wave function and of the entanglement between electronic and nuclei as a function of time. The SVD decomposition leads to a significant compaction of the matricized wave function in terms of a minimum number of separable products of an electronic and nuclear singular vector weighted by singular values arranged in decreasing order. This

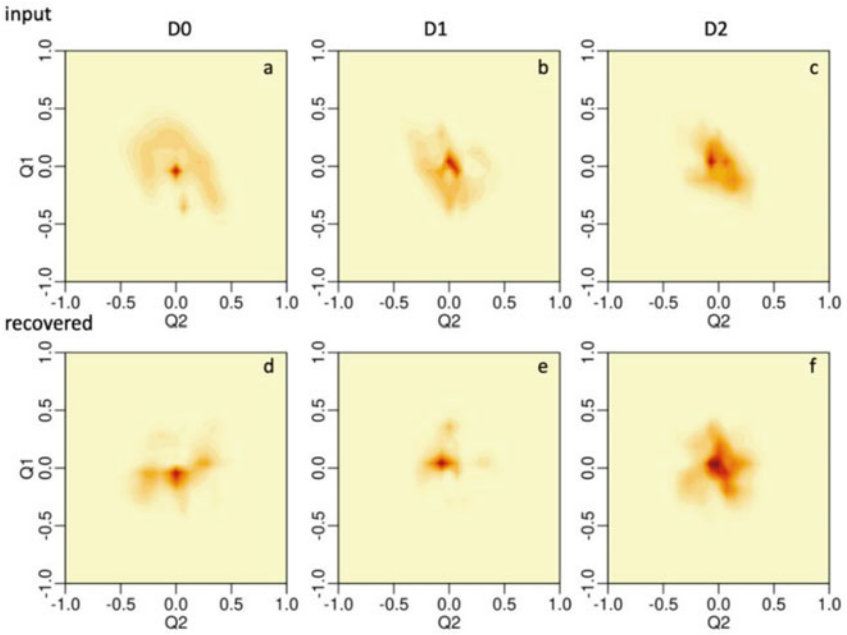

Fig. 8 Top row: Localization of the wave function on the (*q1*, *q2*) grid for the three electronic states D_0(a), D_1(b) and D_2(c) at 0.85 fs, computed by solving the time-dependent Schrödinger equation. Bottom. Recovered localization using 193 separable terms in the HOSVD expansion for D_0(d), D_1(e) and D_2(f)

minimum number of terms corresponds to the Schmidt rank and is significantly smaller than the number of terms of the Born-Huang expansion. The weights of the nuclear and electronic singular vectors on the nuclear and electronic basis sets provide further insights on the physical meaning of the singular components. This analysis can be extended to several nuclear degrees of freedom by HOSVD.

We show that exciting molecules by ultrashort atto and few fs pulses inherently entangles the vibronic wave function because the initial state is a superposition of the several electronic states that fall within the broad energy bandwidth of the pulse. This is unlike excitation with longer pulses where a single electronic state is populated. The entanglement is driven by the nuclear motion. The main contribution to entanglement is the difference in the gradient of the potentials of the different electronic states accessed by the optical pulse. It is therefore possible to control the initial degree of entanglement by exciting specific electronic states using the parameters of the pulse: Its bandwidth, its polarization, its carrier frequency and the carrier-envelope phase for few cycle pulses. The initial entanglement that is controlled by the pulse parameters is further modulated by the non adiabatic interactions which are also driven by nuclear motion. As shown in the case of LiH, these can bring electronic states that were not optically excited in the vibronic wave packet, leading to an increase of the initial entanglement.

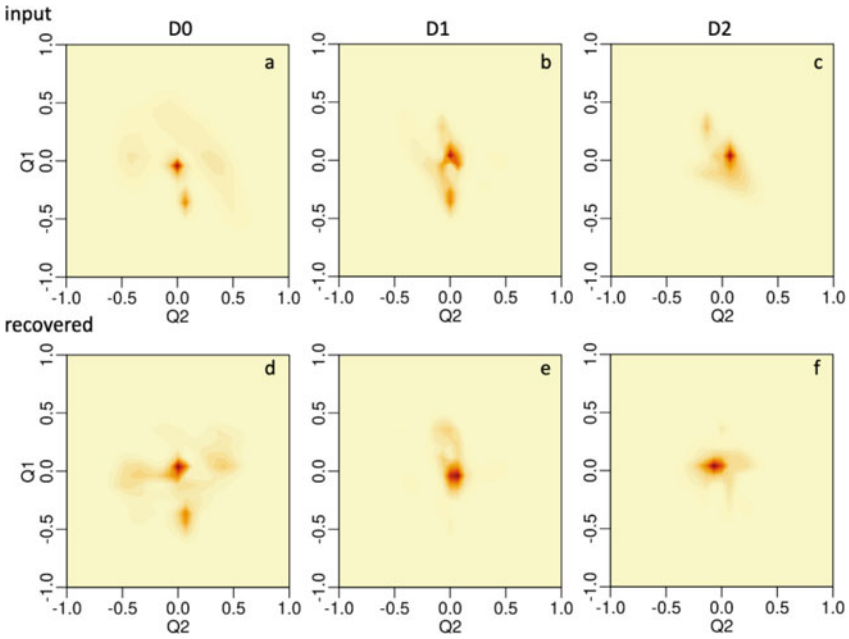

Fig. 9 Top row: Localization of the wave function on the ($q1$, $q2$) grid for the three electronic states D_0(a), D_1(b) and D_2(c) at 1.7 fs, computed by solving the time-dependent Schrödinger equation as described in Ref. [35] Bottom. Recovered localization using 366 separable terms in the HOSVD expansion for D_0(d), D_1(e) and D_2(f)

The compaction of the wave function as a sum of a small number of separable terms opens the way for efficient propagation schemes for the singular states, in connection with recent work based on product matrix states [46–48].

Acknowledgments MB is supported by an Erasmus+ grant between ULiège and HUJI. NG is supported by a joint NSF-BSF project with a BSF award number 2019722. Support from the COST action Attochem(CA18222) is acknowledged. The work of FR and MB is supported by by the Fonds National de la Recherche Scientifique (Belgium), F.R.S.-FNRS, research grant # T.0205.20. Computational resources have been provided by the Consortium des Equipements de Calcul Intensif (CECI), funded by the F.R.S.- FNRS under Grant # 2.5020.11.

References

1. Nisoli, M., Decleva, P., Calegari, F., Palacios, A., Martín, F.: Attosecond electron dynamics in molecules. Chem. Rev. **117**(16), 10760–10825 (2017)
2. Calegari, F., Ayuso, D., Trabattoni, A., Belshaw, L., De Camillis, S., Anumula, S., Frassetto, F., Poletto, L., Palacios, A., Decleva, P., Greenwood, J.B., Martín, F., Nisoli, M.: Ultrafast electron dynamics in phenylalanine initiated by attosecond pulses. Science. **346**(6207), 336–339 (2014)

3. Perfetto, E., Trabattoni, A., Calegari, F., Nisoli, M., Marini, A., Stefanucci, G.: Ultrafast quantum interference in the charge migration of tryptophan. J. Phys. Chem. Lett. **11**, 891–899 (2020)
4. Despré, V., Marciniak, A., Loriot, V., Galbraith, M.C.E., Rouzée, A., Vrakking, M.J.J., Lépine, F., Kuleff, A.I.: Attosecond hole migration in benzene molecules surviving nuclear motion. J. Phys. Chem. Lett. **6**(3), 426–431 (2015)
5. Kling, M.F., Siedschlag, C., Verhoef, A.J., Khan, J.I., Schultze, M., Uphues, T., Ni, Y., Uiberacker, M., Drescher, M., Krausz, F., Vrakking, M.J.J.: Control of electron localization in molecular dissociation. Science. **312**(5771), 246–248 (2006)
6. Kraus, P.M., Mignolet, B., Baykusheva, D., Rupenyan, A., Horný, L., Penka, E.F., Grassi, G., Tolstikhin, O.I., Schneider, J., Jensen, F., Madsen, L.B., Bandrauk, A.D., Remacle, F., Wörner, H.J.: Measurement and laser control of attosecond charge migration in ionized iodoacetylene. Science. **350**(6262), 790–795 (2015)
7. Matselyukh, D.T., Despré, V., Golubev, N.V., Kuleff, A.I., Wörner, H.J.: Decoherence and revival in attosecond charge migration driven by non-adiabatic dynamics. Nat. Phys. **18**, 1206–1213 (2022)
8. Baldini, E., Palmieri, T., Pomarico, E., Auböck, G., Chergui, M.: Clocking the ultrafast electron cooling in Anatase titanium dioxide nanoparticles. ACS Photo. **5**(4), 1241–1249 (2018)
9. Borrego-Varillas, R., Lucchini, M., Nisoli, M.: Attosecond spectroscopy for the investigation of ultrafast dynamics in atomic, molecular and solid-state physics. Rep. Prog. Phys. **85**(6), 066401 (2022)
10. Lucchini, M., Sato, S.A., Lucarelli, G.D., Moio, B., Inzani, G., Borrego-Varillas, R., Frassetto, F., Poletto, L., Hübener, H., De Giovannini, U., Rubio, A., Nisoli, M.: Unravelling the intertwined atomic and bulk nature of localised excitons by attosecond spectroscopy. Nat. Commun. **12**(1), 1021 (2021)
11. Mignolet, B., Levine, R.D., Remacle, F.: Charge migration in the bifunctional PENNA cation induced and probed by ultrafast ionization: a dynamical study. J. Phys. B Atomic Mol. Phys. **47**(12), 124011 (2014)
12. Remacle, F., Nest, M., Levine, R.D.: Laser steered ultrafast quantum dynamics of electrons in LiH. Phys. Rev. Lett. **99**(18), 183902 (2007)
13. Remacle, F., Levine, R.D.: An electronic time scale in chemistry. Proc. Natl. Acad. Sci. U. S. A. **103**(18), 6793–6798 (2006)
14. Valentini, A., van den Wildenberg, S., Remacle, F.: Selective bond formation triggered by short optical pulses: quantum dynamics of a four-center ring closure. Phys. Chem. Chem. Phys. **22**(39), 22302–22313 (2020)
15. Nikodem, A., Levine, R.D., Remacle, F.: Spatial and temporal control of populations, branching ratios, and electronic coherences in LiH by a single one-cycle infrared pulse. Phys. Rev. A. **95**(5), 053404 (2017)
16. Muskatel, B.H., Remacle, F., Levine, R.D.: AttoPhotoChemistry: probing ultrafast electron dynamics by the induced nuclear motion: the prompt and delayed predissociation of N2. Chem. Phys. Lett. **601**(0), 45–48 (2014)
17. Ekert, A., Knight, P.L.: Entangled quantum systems and the Schmidt decomposition. Am. J. Phys. **63**(5), 415–423 (1995)
18. Horodecki, R., Horodecki, P., Horodecki, M., Horodecki, K.: Quantum entanglement. Rev. Mod. Phys. **81**(2), 865–942 (2009)
19. Nielsen, M.A., Chuang, I.L.: Quantum Computation and Quantum Information. Cambridge University Press, Cambridge (2010)
20. Sanz-Vicario, J.L., Pérez-Torres, J.F., Moreno-Polo, G.: Electronic-nuclear entanglement in ${{\mathrm{H}}_{2}}^{+}$: schmidt decomposition of non-born-oppenheimer wave functions expanded in nonorthogonal basis sets. Phys. Rev. A. **96**(2), 022503 (2017)
21. McKemmish, L.K., McKenzie, R.H., Hush, N.S., Reimers, J.R.: Quantum entanglement between electronic and vibrational degrees of freedom in molecules. J. Chem. Phys. **135**(24), 244110 (2011)

22. Haxton, D.J., Lawler, K.V., McCurdy, C.W.: Multiconfiguration time-dependent Hartree-Fock treatment of electronic and nuclear dynamics in diatomic molecules. Phys. Rev. A. **83**(6), 063416 (2011)
23. Haxton, D.J., Lawler, K.V., McCurdy, C.W.: Qualitative failure of a multiconfiguration method in prolate spheroidal coordinates in calculating dissociative photoionization of ${\mathrm{H}}_{2}{}^{+}$. Phys. Rev. A. **91**(6), 062502 (2015)
24. Vatasescu, M.: Entanglement between electronic and vibrational degrees of freedom in a laser-driven molecular system. Phys. Rev. A. **88**(6), 063415 (2013)
25. Izmaylov, A.F., Franco, I.: Entanglement in the born–oppenheimer approximation. J. Chem. Theory Comput. **13**(1), 20–28 (2017)
26. Hou, X.-W., Chen, J.-H., Ma, Z.-Q.: Dynamical entanglement of vibrations in an algebraic model. Phys. Rev. A. **74**(6), 062513 (2006)
27. Li, J., Kais, S.: Entanglement classifier in chemical reactions. Sci. Adv. **5**(8), eaax5283 (2019)
28. Li, J., Sajjan, M., Kale, S.S., Kais, S.: Statistical correlation between quantum entanglement and spin–orbit coupling in crossed beam molecular dynamics. Adv. Quant. Technol. **4**, 2100098 (2021)
29. Vrakking, M.J.J.: Control of attosecond entanglement and coherence. Phys. Rev. Lett. **126**(11), 113203 (2021)
30. Koll, L.-M., Maikowski, L., Drescher, L., Witting, T., Vrakking, M.J.J.: Experimental control of quantum-mechanical entanglement in an attosecond pump-probe experiment. Phys. Rev. Lett. **128**(4), 043201 (2022)
31. Busto, D., Laurell, H., Finkelstein-Shapiro, D., Alexandridi, C., Isinger, M., Nandi, S., Squibb, R.J., Turconi, M., Zhong, S., Arnold, C.L., Feifel, R., Gisselbrecht, M., Salières, P., Pullerits, T., Martín, F., Argenti, L., L'Huillier, A.: Probing electronic decoherence with high-resolution attosecond photoelectron interferometry. Eur. Phys. J. D. **76**(7), 112 (2022)
32. Blavier, M., Levine, R.D., Remacle, F.: Time evolution of entanglement of electrons and nuclei and partial traces in ultrafast photochemistry. Phys. Chem. Chem. Phys. **24**(29), 17516–17525 (2022)
33. Blavier, M., Gelfand, N., Levine, R.D., Remacle, F.: Entanglement of electrons and nuclei: amost compact representation of the molecular wave function. Chem. Phys. Lett. **804**, 139885 (2022)
34. Bradley, T.-D., Stoudenmire, E.M., Terilla, J.: Modeling sequences with quantum states: a look under the hood. Mach. Learn.: Sci. Technol. **1**(3), 035008 (2020)
35. Blavier, M., Komarova, K., Gonçalves, C.E.M., Levine, R.D., Remacle, F.: Electronic coherences steer the strong isotope effect in the ultrafast Jahn–teller structural rearrangement of methane cation upon tunnel ionization. J. Phys. Chem. A. **125**(43), 9495–9507 (2021)
36. van den Wildenberg, S., Mignolet, B., Levine, R.D., Remacle, F.: Temporal and spatially resolved imaging of the correlated nuclear-electronic dynamics and of the ionized photoelectron in a coherently electronically highly excited vibrating LiH molecule. J. Chem. Phys. **151**(13), 134310 (2019)
37. Ajay, J.S., Komarova, K.G., Remacle, F., Levine, R.D.: Time-dependent view of an isotope effect in electron-nuclear nonequilibrium dynamics with applications to N2. Proc. Natl. Acad. Sci. U. S. A. **115**, 5890–5895 (2018)
38. Golub, G.H., Reinsch, C.: Singular value decomposition and least squares solutions. In: Wilkinson, J.H., Reinsch, C., Bauer, F.L. (eds.) Linear Algebra, pp. 134–151. Springer, Berlin/Heidelberg (1971)
39. Baker, S., Robinson, J.S., Haworth, C.A., Teng, H., Smith, R.A., Chirilă, C.C., Lein, M., Tisch, J.W.G., Marangos, J.P.: Probing proton dynamics in molecules on an attosecond time scale. Science. **312**(5772), 424–427 (2006)
40. Marangos, J.P., Baker, S., Kajumba, N., Robinson, J.S., Tisch, J.W.G., Torres, R.: Dynamic imaging of molecules using high order harmonic generation. Phys. Chem. Chem. Phys. **10**(1), 35–48 (2008)
41. Mondal, T., Varandas, A.J.C.: The Jahn-teller effect in the triply degenerate electronic state of methane radical cation. J. Chem. Phys. **135**(17), 174304 (2011)

42. Mondal, T., Varandas, A.J.C.: On extracting subfemtosecond data from femtosecond quantum dynamics calculations: the methane cation. J. Chem. Theory Comput. **10**(9), 3606–3616 (2014)
43. Mondal, T., Varandas, A.J.C.: Structural evolution of the methane cation in subfemtosecond photodynamics. J. Chem. Phys. **143**(1), 014304 (2015)
44. Gonçalves, C.E.M., Levine, R.D., Remacle, F.: Ultrafast geometrical reorganization of a methane cation upon sudden ionization: an isotope effect on electronic non-equilibrium quantum dynamics. Phys. Chem. Chem. Phys. **23**(21), 12051–12059 (2021)
45. Zhang, T., Golub, G.H.: Rank-one approximation to high order tensors. Siam J. Matrix Anal. Appl. **23**(2), 534–550 (2001)
46. Baiardi, A., Reiher, M.: Large-scale quantum dynamics with matrix product states. J. Chem. Theory Comput. **15**(6), 3481–3498 (2019)
47. Larsson, H.R., Zhai, H., Gunst, K., Chan, G.K.-L.: Matrix product states with large sites. J. Chem. Theory Comput. **18**(2), 749–762 (2022)
48. Schollwöck, U.: The density-matrix renormalization group in the age of matrix product states. Ann. Phys. **326**(1), 96–192 (2011)